Partial-Composite Behavior of Sandwich Beams Composed of Fiberglass Facesheets and Woven Fabric Core

Aidan McCracken and Pedram Sadeghian[1]

Department of Civil and Resource Engineering, Dalhousie University, 1360 Barrington Street, Halifax, NS, B3H 4R2, Canada.

Abstract:

In this study, thin-walled sandwich composites made of glass fiber-reinforced polymer (GFRP) facesheets and a three-dimensional (3D) woven fabric core were studied. A total of 30 small-scale sandwich beam specimens were manufactured across six unique beam varieties with dimensions of 50 mm in width, and 200 or 350 mm in length to be tested under four-point bending up to failure. The load-deflection behavior, load-strain behavior, moment-curvature behavior, and neutral axis location were analyzed. Based on the test results, the flexural stiffness, shear stiffness, core shear modulus of the sandwich beams were calculated. Also, an analytical model is presented to consider the effect of core shear modulus on deformation and composite action of the test specimens. The model is capable to quantify the degree of composite action based on the geometry and material properties of sandwich beams. Overall, the sandwich beams displayed a partial-composite behavior raging from 15 to 91% of full-composite behavior, which was a function of the relative stiffness of the facesheets and the core plus the length of the shear span. It was shown that compatibility between the mechanical properties of the facesheet and core is a key factor in optimizing sandwich panels made of the core. The results will be used for the design of thin-walled

[1] Corresponding Author: Pedram.Sadeghian@dal.ca

sandwich liners for the rehabilitation of underground infrastructure including existing highway culverts and large diameter drainage systems.

https://doi.org/10.1016/j.tws.2018.08.003

Keywords: Woven fabric; core; sandwich; composite action; flexural stiffness.

1. INTRODUCTION

The use of sandwich structures are increasing as engineers look to maximize the efficiency of structures and to minimize their weight. Sandwich composites made of fiber-reinforced polymer (FRP) facesheets and lightweight, low-density core materials have been shown to be effective in reducing weight and increasing strength and stiffness in a variety of structural applications. The FRP facesheets resist the tensile and compressive stresses due to bending, while the core resists shear stresses, provides insulation, and increases the distance between facesheets resulting in an increased moment of inertia. Sandwich panels are often favored in high-performance structural applications due to their relatively light weight and high moment of inertia [1]. The use of various FRP facesheet materials such as fiberglass and carbon [2][3] as well as natural fibers such as flax [4] have been studied. Also, a variety of core materials have been explored for use in composite sandwich beams and panels. Foam materials have commonly been studied for sandwich composites providing a continuous core between the facesheets [5][6][7]. This study focusses on discrete core materials, particularly on woven core systems. The mechanics of sandwich beams and plates with discrete core have been investigated for various materials and core geometries, i.e. web-core, honeycombs, corrugated core, C- and Z-cores, etc. over last decades. Also, different materials have been considered ranging from metals to composites.

Three-dimensional (3D) woven fabrics have more recently been introduced and provide a viable alternative in sandwich construction [8][9][10][11][12]. Typically, 3D woven fabrics are manufactured multi-layered warp fibers in the structured direction, and two orthogonal sets of weft fibers which interlace with the warp fibers to provide structural stability in all directions [13]. These core materials provide a new generation of sandwich structures with a high facesheet to core debonding strength and reducing the weight and cost of the structure [14][15]. There is a large variety in possible core layouts and thus mechanical performance [16]. Numerous studies have previously been conducted on the failure mechanisms of sandwich composites with 3D fabric cores [17][18][19][20][21][22][23][24]. Furthermore, the dynamic behavior [25][26], damping properties [27], and impact performance [28][29] of the 3D core sandwich system have been studied. It has been shown that the mechanical properties of 3D core sandwich structures are significantly affected by the configuration of the woven core. Consequently, various styles of multi-dimensional cores must be studied to enhance strength and predictability surrounding sandwich composites manufactured with a 3D woven fabric core.

As compared to conventional core materials such as foam and honeycomb, a 3D fabric core may provide many significant manufacturing advantages. As the material is provided as a fabric, it is initially very flexible and can be used easily as a core in non-conventional applications such as curved surfaces and tubular sandwich structures. Whereas conventional cores may need to be cut to accommodate smaller radii, a 3D fabric can simply be rolled into place before the curing process. Furthermore, as the composite facesheets and core are cured at the same time, they will ideally have an improved structural unity and this may eliminate the risk of debonding and delamination, which is a common issue in sandwich panel construction [30][31]. Moreover, since

3D fabric comes in a roll, it is a very easy to transport material and long lengths of composite beams can be produced without any seams or overlap in the core.

In this paper, glass FRP (GFRP) facesheets are combined with a 3D woven fabric core to manufacture sandwich beams with zero, one and two layers of GFRP facesheets. In the manufacturing of these panels, both the facesheets and core were cured using the same epoxy resin at the time. The aim of the study is to analyze and evaluate the structural performance of sandwich beams consisting of GFRP facesheets in combination with a singular style of 3D fabric core. Based on existing information, it can be concluded that 3D fabric holds great potential in the world of sandwich composites. As new fabrics are manufactured exclusively for structural purposes, their structural performance must be evaluated. In this study, multiple small-scale sandwich beams were manufactured and tested under four-point bending. Structural properties such as strength and stiffness as well as core properties such as shear modulus are evaluated. Moreover, the interaction between the GFRP facesheets and the 3D fabric core is analyzed. Additionally, an analytical model is developed to calculate and predict the degree of full-composite behavior of the sandwich composites.

2. RESEARCH SIGNIFICANCE

This research is a part a project on application of thin-walled sandwich composite liners for rehabilitation of underground infrastructure including existing highway culverts and large diameter water/wastewater systems. Rather than applying layers after layers of expensive FRPs to achieve required thickness of a solid liners, a sandwich FRP system can be applied in place to achieve the same strength and stiffness of the solid liner. Since dry 3D fabrics are flexible, it is a very easy to saturate them in place and apply them on the inner surface of the culvert after a few

layers of FRP layers and then apply a few layers of FRPs forming a sandwich liner with minimum expensive FRP materials. This paper focuses on the characterization of the 3D core using flat sandwich beams before moving forward with using the 3D core for a curved-shape sandwich liner. The key point is the flexibility of dry 3D fabric to accommodate the shape of the liner based on the actual shape and dimension of the existing culvert/pipe without a significant reduction of the cross-section of the culvert/pipe affecting the hydraulic of the system negatively. Other core materials such as honeycomb and foam core materials are not able to accommodate the required curvature. The outcomes of this research will help to find more sustainable and cost-effective solutions for aging underground infrastructure around the world.

3. EXPERIMENTAL PROGRAM

3.1. Test Matrix

A total of 30 sandwich specimens with a three-dimensional (3D) woven fabric core were fabricated to be tested under four-point bending. The variables were the number of layers of facing as well as the specimen span. Two different span lengths, 150 mm and 300 mm were tested. The long span was selected to ensure the sandwich beams will reach to failure without excessive deflections beyond the stroke capacity of the testing machine. The short span was selected to have two sets of load-deflection behaviors required for calculation of flexural and shear stiffness of the sandwich beams as it will be explained later. All specimens had an 8-mm nominal thick 3D woven fabric core and had either 1 or 2 layers of GFRP facesheet. As the 3D fabric had its own top and bottom facesheets, stiff enough to be considered as test specimens. So, a group of specimens were made without GFRP facesheets. Then 1 and 2 layers of GFRP facesheets were added as reinforcement of the 3D core. The test matrix is shown in Table 1. Five identical specimens were made for each

case. The test specimens are identified with a specimen ID such as GX-SY where G stands GFRP, S stands for span, X identifies the number of GFRP facesheet layers and Y identifies the span length in mm. For example, G0-S150 is a 3D fabric core sandwich beam with zero (0) layers of GFRP facesheet tested with a 150-mm span.

3.2. Material Properties

For the GFRP facesheets, a 915 g/m^2 (gsm) unidirectional fiberglass fabric was used. The fabric was made of glass fibers with a density of 2.55 g/cm^2, a tensile strength of 3.24 GPa, an elastic modulus of 72.4 GPa and a rupture strain (ultimate elongation) of 4.5% all as reported by the manufacturer (QuakeWrap Inc., Tucson, AZ, USA) for the dry fibers. For making the sandwich composites, a two-component epoxy resin mixture was used. The resin mixture comes in two parts: an epoxy and a hardener which are mixed in a 2:1 by-volume ratio respectively. The epoxy and hardener are reported to have densities of 1.13 kg/L and 1.00 kg/L respectively. This gives a density of 1.087 kg/L for the liquid resin when mixed in the specified ratio. Five samples of cured resin were created to compare the reported liquid density to a solid density. Across five samples, an average solid resin density was found to be 1.13 kg/L with a standard deviation of 0.04 kg/L. The resin, having been cured at room temperature for 48 hours, was reported by the manufacturer to have a tensile strength of 49.3 MPa, a compressive strength of 65.4 MPa, and a tensile elastic modulus of 1995 MPa.

Five identical GFRP tensile coupons made of two layers of the unidirectional fabric and epoxy resin were prepared using wet hand lay-up method and tested according to ASTM D3039 [32]. The overall dimension of the coupons was 25 mm x 250 mm with two tabs attached on both sides on each end of the coupon. The tabs were made of the same GFRP material and had dimensions of 25 mm x 125 mm. These tabs were used to aid in the gripping of the coupon during

the test and to ensure that the gripping did not produce any stress concentrations or premature failures. The tab dimensions are shown in Figure 1. A 100 kN universal testing machine with a displacement rate of 2 mm/min was used. A strain gauge was applied on each side of the coupons, centered in the longitudinal direction of fibers/coupon to measure the axial strain. Figure 1 shows the tensile test results based on the nominal ply thicknesses of 1.3 mm as reported by the manufacturer. The average tensile strength of the GFRP coupons was 583 MPa with a standard deviation of 31 MPa. As shown in Figure 1, the GFRP coupons displayed a nearly linear behavior up to the point of rupture. The average elastic modulus of the GFRP coupons was 21.75 GPa with a standard deviation of 0.58 GPa.

Using the nominal areal weight of 915 gsm (1830 gsm for two layers of fiberglass), the fiber weight fraction (FWF) of the GFRP coupons was calculated. The coupons had an average FWF of 0.52 (thus, 52% of the mass is contributed by fibers) with a standard deviation of 0.03. Using the role of mixture [33], the fiber volume fraction (FVF) can be calculated as a function of the FWF, the density of the dry fiberglass (ρ_f), and the density of the matrix (ρ_m) as presented in Eq. (1). The density of the dry fiberglass was reported to be 2.55 g/cm^3 and the solid matrix density was calculated to be 1.13 g/cm^3 as explained previously. The average FVF of the coupons was calculated as 0.327 with a standard deviation of 0.026.

$$\rho_f \left(\frac{1}{FWF} - 1\right) = \rho_m \left(\frac{1}{FVF} - 1\right) \quad (1)$$

For the core of the sandwich specimens, a 3D woven fabric was used. The 3D fabric consists of two bi-directional woven fiberglass fabric surfaces, which are mechanically connected with vertical woven piles. Two S-shaped piles combine to form a pillar, 8-shaped in the warp direction and 1-shaped in the weft direction. The fabric comes in a flexible roll and when cured with the epoxy resin it rises and stiffens into its full thickness. The manufacturer reported the areal

weight of 1050 gsm and thickness of 8 mm for the 3D core. Other properties of the core include: density of warp = 15 ends/cm, density of weft = 8 ends/cm, warp tensile strength = 6,000 N/50mm, and weft tensile strength = 10,000 N/50mm. Across 9 samples of the core after curing, an actual average thickness was found to be 7.54 mm. Figure 2(c) shows a cross-sectional view of a cured sample of 3D core. Note that after curing, the core remains hollow as the resin does not clog any of the cells. The dry 3D core was measured to have a weight of approximately 1050 gsm as reported by the manufacturer. When cured with the resin, the 3D fabric composite was measured to have an average weight of 2988 gsm with a standard deviation of 134 gsm. Accordingly, the 3D fabric composite specimens had an average FWF of 0.352 with a standard deviation of 0.017. Using the actual thickness of 7.54 mm of cured 3D fabric, the bulk density of dry and cured 3D fabric was calculated as 139 and 396 kg/m^3, respectively.

3.3. Specimen Fabrication

When producing the sandwich specimens, sheets of both fiberglass and 3D fabric (approximately 400 mm x 635 mm) were carefully cut using shears. Originally creating large panels allowed for a greater quantity of specimens to be manufactured at once. All specimens were fabricated using the wet lay-up method. Brushes and a roller were used to distribute the resin across the surface of the fabric and a spatula was used to smooth the layer of resin. To ensure that the 3D fabric core had enough resin, both sides of the fabric sheet were pre-saturated before applying it to the surface of the already saturated fiberglass facesheet. The specimens were prepared on a layer of parchment paper. Furthermore, an additional layer of parchment paper was applied to the top surface of the specimens as they cured for approximately 48 hours at room temperature. Parchment paper allowed the outer surfaces of the specimens to have a smooth and consistent finish. This style of

production provided one large panel of the composite, which was then cut into the sandwich beams using a diamond-bladed saw after the curing process was complete.

The composite panels were first cut into 50 mm wide strips. This was followed by them cutting them into either 200 mm or 350 mm long beams as shown in Figure 3. An overhang length of 25 mm was considered at each support of the beam specimens. Thus, 200 mm and 350 mm long specimens had an actual span of 150 mm and 300 mm, respectively. A digital caliper was used to measure the width and thickness of each specimen at three locations for further calculations. It should be noted that the flexural and shear strength of the 3D fabric core in the weft direction are higher than those in the warp direction. However, authors only investigated the warp direction behaviors of the core as the core was intended to be used later for wrapping around a mandrel to manufacture pipes and test them using the parallel-plate compression method. As a result, the warp direction of the core in the circumferential direction of the pipe was the point of interest.

3.4. Test Set-up and Instrumentation

For the sandwich beam testing, a four-point bending setup was used for all specimens with a different loading span proportional to the supporting span as shown in Figure 4. The loading span (L) was equal to (2/11) of the supporting span (S) per ASTM D7249 [34] and ASTM D7250 [35]. In terms of instrumentation, each specimen had two strain gauges at mid-span applied on the top and bottom in the longitudinal direction to measure the compressional and tensile strains, respectively. Additionally, two linear potentiometers (LPs) were placed directly in the middle of the span to measure the average mid-span deflection of the beams. Due to the size of the testing machinery, the LPs were not able to fit directly underneath the beams. Consequently, a thin and rigid piece of steel was secured to the bottom of the beams to keep contact with the tip of the LPs; this steel did not affect the response of the beam and moved downward along with the bottom of

the beam. All tests were done with a 100 kN universal testing machine and were displacement controlled with a fixed rate of 2 mm/min.

4. RESULTS AND DISCUSSIONS

A summary of the test results as well as the mode of failure for each case is shown in Table 2.

4.1. Modes of Failure

As seen in Table 2, there were three different modes of failure observed during testing. The three modes of failure were crushing of the core facing (G0 specimens), core transverse shear failure (G1 specimens), and core longitudinal shear failure (G2 specimens). Although the zero-, one- and two-layer specimens were controlled by a different mode of failure, it was the core that failed first each time. Thus, regardless of the facesheet thickness or strength, the core material is what limits the strength of these composite sandwich beams. As discussed, this behavior is expected in sandwich composites. In the specimens with one and two layers of GFRP facesheet, no indentation, buckling, or tensile rupture of the facesheets were observed. All three modes of failure can be seen in Figure 5.

An interesting observation during testing was how the core seemed to behave differently with one layer of facing (G1 specimens) in comparison to two layers (G2 specimens). During the one-layer tests, the vertical fibers of the core remained almost vertical as the core deformed due to transverse shear. During the two-layer tests, the same vertical fibers were forced to tilt diagonally due to the dominant longitudinal shear. This difference can be seen in detail in Figure 6 along with a schematic comparing the two behaviors. It is hypothesized that the longitudinal core shear failure is due to significant partial-composite behavior of specimens with two layers facing. This means

that the core was not rigid enough to maintain a linear strain profile in the specimens with two-layer GFRP facings, which were twice as stiff compared to one-layer GFRP facings.

The partial-composite behavior can be explained using the Timoshenko beam theory, rather than the common Euler-Bernoulli beam theory. The schematic shown in Figure 6 illustrates the main visual difference between the two theories. The Euler-Bernoulli theory assumes that the beams cross-section remains perpendicular to the bending line while the Timoshenko theory allows for rotation due to shear deformation. When the shear deformation is small, Euler-Bernoulli theory approaches Timoshenko theory. In terms of sandwich beams, Euler-Bernoulli is an accurate model of the beam's behavior when the core has adequate stiffness/strength in both the transverse and longitudinal directions. The concept of partial-composite action is further described in the analytical section.

The failure modes observed in this study are compatible with the tests performed by Hu et. al [24], who tested 3D woven fabrics with and without strengthening facesheets under three-point bending. It was observed that the 3D fabric beams without strengthening facesheets failed under bending with crushing of the fabric similar to G0 specimens in the current study. Moreover, the 3D fabric beams with strengthening facesheets were failed under shear (Mode A and Mode B). The shear failure Mode B was observed in specimens with long shear spans where the core was shifted vertically similar to G1 specimens in the current study. The shear failure Mode A was observed in specimens with short shear span where top and bottom facesheets were shifted horizontally similar to G2 specimens in the current study.

4.2. Load-Deflection Behavior

Figure 7 shows the average load-deflection behavior for the zero-, one- and two-layer sandwich beams. Figure 7(a) and 7(b) display the behavior for the spans of 150 mm and 300 mm,

respectively. Five identical specimens were tested per case and the average results were plotted. The zero-layer specimens displayed linear behavior up to the point of instant failure due to crushing of the 3D core. The one- and two-layer specimens displayed a section of linearity followed by a slowly ascending curve up to a peak load, as shown in Figure 7. As expected, the initial stiffness and peak load for both span lengths of the beams with zero layers of GFRP facesheets was substantially less than the one- and two-layer specimens. However, it is notable that the one-layer beams displayed a higher initial stiffness for both span lengths. This is theorized to be caused by the partial-composite behavior by the two-layer specimens, which is further described in the analytical section. Since the strength of the facesheets is much higher than the strength of the core, the facesheets begin to behave independently. Thus, due to bending, the two facesheets begin to shift longitudinally with respect to each other, developing a longitudinal shear stress in the core. As the facesheet thickness increases, the longitudinal stiffness of the facesheet increases. This increases the normal stress in the facesheet and subsequently increases the longitudinal shear stress in the core. As the core is softer and weaker in the longitudinal direction compared to the vertical direction, the longitudinal shear deformation of the core governs the behavior of the two-layer specimens. Accordingly, this weakness in the longitudinal direction of the core coupled with the increase in longitudinal shear stress may explain in the relative weakness of the two-layer specimens. This behavior can be explained using the Timoshenko beam theory where plane sections do not remain plane throughout bending, as shown in Figure 6.

4.3. Load-Strain Behavior

Figure 8 illustrates the average load-strain behavior for the zero-, one- and two-layer sandwich beams. Figure 8(a) and 8(b) display the behavior for the spans of 150 mm and 300 mm, respectively. As seen in Figure 8, the G1 and G2 specimens displayed very similar initial load-

strain behavior which indicates a similar initial elastic modulus. In terms of the 150 mm specimens, the G2 specimens displayed interesting behavior. Although the initial behavior was similar to the G1 specimens, at a load of approximately 1200 N the core began to fail due to longitudinal shear. However, this did not result in the beam failing instantly. Rather, it was followed by a section with a flatter strain profile before the beams failed at an average load of 1572.9 N. In comparison, the G1 specimens displayed a relatively linear behavior before failing at an average load of 1424.6 N.

As seen in the previous section, the 300-mm span specimens reached an average peak load of 1323.9 N and 628.3 N for the G1 and G2 specimens, respectively. Although it would be expected that the G2 specimens would display a higher stiffness and a higher peak load, the interaction between the stiff/strong facesheets and the soft/weak core compromised the structural performance of the sandwich beams. The effects of the partial-composite behavior are more evident when considering the shorter span length of 150 mm as shear is more dominant than bending.

4.4. Moment-Curvature Behavior

The curvature of each specimen was calculated based on the slope of strain profile at mid-span. The strain profile was assumed linear and obtained using the tensile and compressive strains of facesheets using strain gauges. Figure 9 presents the average moment-curvature behavior for the zero-, one- and two-layer sandwich beams. Figure 9(a) and 9(b) display the behavior for the spans of 150 mm and 300 mm, respectively. As seen in Figure 9(a), the moment-curvature behavior of the G1 and G2 specimens with a span of 150 mm was essentially identical. Thus, the flexural stiffness of the two beam types was the same, based on experimental calculations from the moment-curvature behavior. Although the G2 specimens displayed a slightly higher flexural stiffness than the G1 specimens, they failed at a much lower value of moment and curvature. This

is again a result of the partial-composite behavior as the core failed due to longitudinal shear in the G2 specimens at a much lower load than the G1 specimens, which failed due to transverse shear. Although the lower load indicates a different failure mode, the lower than expected values for flexural stiffness of the G2 beams confirms that the partial-composite behavior affects the behavior, regardless of the applied load. The slope of the linear section of the moment-curvature of each specimen was calculated and results are presented in Table 2. The slope represents the flexural stiffness (*EI*) of the specimens and will be discussed further in the analytical section.

4.5. Neutral Axis Location

The location of neutral axis of each specimen was calculated based on tensile and compressive strains and assumption of linear strain profile. Figure 10 shows the average neutral axis location for the zero-, one- and two-layer sandwich beams plotted with respect to moment. Figure 10(a) and 10(b) display the behavior for the spans of 150 mm and 300 mm, respectively. In Figure 10, a neutral axis location of 0 mm indicates that the neutral axis remained exactly in the middle of the beam's cross section. The neutral axis location remained approximately in the middle of the cross section for the G1 and G2 specimens. However, the data for the G0 specimens was less consistent. This could be due to crushing and indentation of the core caused by the loading apparatus as well as the supports.

4.6. Flexural Stiffness and Shear Stiffness

In this section, the flexural stiffness *EI* (known as *D*) and the shear stiffness *GA* (known as *U*) of the specimens is calculated based on the method presented by ASTM D7250 [35], which provides a standard method of determining flexural and shear stiffness and core shear modulus using calculations involving measured deflections of sandwich specimens. Tests can be conducted on short specimens and on long specimens as performed in the experimental section of this study.

Then the flexural stiffness and shear stiffness can be determined by simultaneous solution of the complete deflection equations for each span based on the superposition of the elastic flexural and shear deformations as follows:

$$\Delta = \frac{P(2S^3 - 3SL^2 + L^3)}{96D} + \frac{\mathrm{P(S - L)}}{4U} \quad (2)$$

where Δ is the total mid-span deflection, P is the load, S is total span, and L is the loading span under four-point bending condition. Using the experimental values of the initial stiffness K of two span lengths of each group of specimens obtained from linear portion of each specimen's load-deflection curve, Equation (2) is rearranged as follows:

$$K_i \frac{2S_i^3 - 3S_iL_i^2 + L_i^3}{96D} + K_i \frac{S_\mathrm{i} - L_i}{4U} = 1 \quad (3)$$

where K_i is initial stiffness in N/mm, S_i is the span length in mm and L_i is the loading span in mm. Note that all occurrences of subscript i denotes that this is a value that is specific to each span length. For example, S_1 represents the span length of 150 mm while S_2 represents the span length of 300 mm. Combining the equations for each span length, solving for D and U, and simplifying gives:

$$D = \frac{m_2n_1 - m_1n_2}{96(\frac{n_1}{K_2} - \frac{n_2}{K_1})} \quad (4)$$

$$U = \frac{m_1n_2 - m_2n_1}{4(\frac{m_1}{K_2} - \frac{m_2}{K_1})} \quad (5)$$

where

$$m_i = 2S_i^3 - 3S_iL_i^2 + L_i^3 \quad (6)$$

$$n_i = S_i - L_i \quad (7)$$

Using the experimental initial stiffness values for the 150 mm and 300 mm spans, values for D and U were calculated using Equations (4) and (5), respectively. In this case, values were

calculated using S_1 = 150 mm and S_2 = 300 mm. Additionally, values for *D* were calculated by determining the initial slope of the moment-curvature curves. Table 3 displays both calculated values for the flexural stiffness D for G0, G1, and G2 sandwich beams as well as the calculated values for the shear stiffness *U*. It also presents the average flexural stiffness *D* of each sandwich beam specimen calculated based on the slope of the linear zone of the moment-curvature diagram of the test specimens.

Figure 11 visually illustrates the compared values for flexural stiffness. Although theoretically the values should be equal for beams with identical cross sections, there is a notable discrepancy between the two values of *D* calculated for the G1 specimens. A visual comparison of the calculated flexural stiffness values is shown in Figure 11. Also, Figure 12 illustrates the variation in shear stiffness between the G0, G1, and G2 specimens calculated using Equation (5). Additionally, the average of these three values is displayed on the diagram. It indicated that the shear stiffness does not change with adding GFRP facesheets.

4.7. Core Properties

Figure 13 illustrates a schematic of a typical sandwich beam cross section with important dimensions labelled. In this case, *b* is the width of the beam, *t* is the facesheet thickness, *c* is the core thickness, *d* is the distance measured from the center of each facesheet, and *h* is the height of the entire composite sandwich beam. All dimensions have units of mm for further calculations. The core shear modulus G_c can thus be calculated by the following equation:

$$G_c = \frac{U(h-2t)}{(h-t)^2 b} \tag{8}$$

Figure 14 displays the variation in core shear modulus for the G0, G1, and G2 specimens calculated using Equation (8). As seen in Figure 14, the core shear modulus decreased slightly with each layer of GFRP facesheet added. The sandwich beams had an average core shear modulus

of 16.60 MPa. It should be noted that the compression modulus of the core can be determined using compression testing, which is out of the scope of this paper.

Sadeghian et al. [4] had previously studied the properties of sandwich beams manufactured with GFRP facesheets and a polypropylene honeycomb core with an average core density of 100 kg/m^3 before applying resin. Honeycomb thicknesses of 6 mm and 12 mm were shown to have an average shear stiffness U of 6.2 kN and 9.2 kN and an average core shear modulus G_c of 13.9 GPa and 11.8 GPa, respectively. In this study, the 3D fabric core with an average density of 139 kg/m^3 (before applying resin) displayed an average shear stiffness U of 7.96 kN and an average core shear modulus G_c of 16.60 GPa. The results indicate that the 3D fabric core used in this study had comparable and even higher shear rigidity and modules properties. However, the number of GFRP facesheet layers should be limited to ensure there is a compatibility between the facesheets and the core. More research on larger scale specimens made of thicker 3D fabric cores is needed to generalize the result of this study.

5. ANALYTICAL STUDY

In this section, an analytical approach is implemented to predict the experimental results independently. The analytical approach considers the effect of facesheet thickness and overhang length on the flexural stiffness of the sandwich beams made of 3D fabric core, where the partial-composite action is significant as observed in the experimental study.

5.1. Full-Composite Action

It is well-known that bending of a sandwich beam with thin facesheets and rigid enough core can be formulized based on Euler-Bernoulli beam theory. In this case, the facesheets and the core deform under full-composite action in which the strain profile remains perpendicular to the axis of

the beam. Consider a sandwich beam with the cross-section as shown in Figure 13. The cross-section has a width *b* and total thickness *h*. Each facesheet has thickness *t* and the two facesheets are separated by a relatively thick core of thickness *c*. It is assumed that all three layers are perfectly bonded together and plane section remains plane and perpendicular to the axis of the beam. As a result, the sandwich beam behaves as abeam with full-composite action. Therefore, its flexural stiffness *D* is the sum of the flexural stiffness of both facesheets and the core, measured about the centroidal axis of the cross-section as follows:

$$D = E_f \frac{bt^3}{6} + E_f \frac{btd^2}{2} + E_c \frac{\mathrm{bc}^3}{12} \tag{9}$$

where E_f and E_c are the elastic modulus of facesheet and core, respectively, and d is the distance between the center lines of the upper and lower facesheets. The third term at the right-hand side of Equation (9) is typically ignored indicating the contribution of the core to *D* is neglected [5]. As a result, the flexural stiffness can be presented as follows:

$$D = E_f \left(\frac{bt^3}{6} + \frac{\mathrm{btd}^2}{2} \right) = E_f \left(I_f + \frac{\mathrm{btd}^2}{2} \right) = E_f I \tag{10}$$

where I_f is the some of the moment of inertia of facesheets about their own centroidal axes and *I* is the moment of inertia of facesheets about the centroidal axis of the sandwich beam. The above-mentioned formulation is valid for sandwich beams with thin facesheets acting as thin membranes with insignificant local flexure about their own centroidal axes. The next section describes cases with thick facesheets, where full-composite action is not applicable.

5.2. Partial-Composite Action

In sandwich beams with thick facesheets, the contribution of the local flexural stiffness of facesheets (i.e. $E_f I_f$) to the flexural stiffness of the sandwich beam (i.e. $E_f I$) is significant. As a result, a flexible core is not able to maintain the full-composite action of the sandwich beam per

the Euler-Bernoulli beam theory. As shown in Figure 6(c), the partial-composite action also affects the shear deformation of the core according to the Timoshenko beam theory. Allen [5] formulized this phenomenon for a sandwich beam under four-point bending as presented in Figure 15. It should be noted that the thick facesheets solution is more general than the thin facesheets solution. With the thick facesheets solution approaches to the thin facesheets solution, the partial-composite action decreases and approaches to the full-composite action, where Eq. (9) is applicable. Otherwise, the facesheets behave partially independent causing more flexible and weaker sandwich beam than a sandwich beam with thin facesheets.

The four-point bending test method is the most common test method to determine the flexural stiffness of sandwich beams as it was used in the current study. The reason is the assumption of no shear force and subsequently no shear deformation in the central region. This assumption is true for sandwich beams with thin facesheets and stiff cores. However, the assumption is not valid for sandwich beams with thick facesheets and flexible cores. Per Allen [5], the total deflection *w(x)* at any point *x* from the mid-span in the central region of the beam shown in Figure 15 can be expressed as follows:

$$w(x) = \frac{PL_b}{4}\frac{x^2}{E_f I} + \frac{\beta P}{2\alpha^3 E_f I_f}(cosh\ \alpha x - 1)\left(1 - \frac{I_f}{I}\right) \tag{11}$$

where P is the total load and L_b is shear span as shown in Figure 15. The parameter α represents the ratio of the shear stiffness $U=G_cA$ to the local flexural stiffness of the facesheets as follows:

$$\alpha^2 = \frac{G_c A}{E_f I_f\left(1 - \frac{I_f}{I}\right)} \tag{12}$$

where G_c is the core shear modulus and $A=bd^2/c$ is the effective shear area. The factor β is defined as follows:

$$\beta = \frac{\sinh \alpha(L_b + L_c) - \sinh \alpha L_c}{\cosh \alpha(L_a + L_b + L_c)} \tag{13}$$

where L_a, L_b, and L_c are the lengths shown in Figure 15. The flexural stiffness D' of a sandwich beam with thick facesheets considering partial-composite action of facesheets can be calculated as follows:

$$D' = \frac{PL_b x^2}{4w(x)} \tag{14}$$

The partial-composite flexural stiffness D' can be compared to the full-composite flexural stiffness D as follows:

$$k = \frac{\frac{1}{D'} - \frac{1}{D}}{\frac{1}{D}} = \frac{2\beta}{\alpha L_b}\left(\frac{cosh\ \alpha x - 1}{\alpha^2 x^2}\right)\left(\frac{I}{I_f} - 1\right) \tag{15}$$

where k is the fractional error in $1/D'$. As x approaches to zero (i.e. mid-span), the fractional error k is simplified as follows:

$$k = \frac{\beta}{\alpha L_b}\left(\frac{I}{I_f} - 1\right) \tag{16}$$

Finally, the partial-composite flexural stiffness D' for a sandwich beam can be obtained from following equation:

$$D' = \frac{1}{k+1} D = \frac{1}{k+1}\left(E_f \frac{bt^3}{6} + E_f \frac{\mathrm{btd}^2}{2} + E_c \frac{\mathrm{bc}^3}{12}\right) \tag{17}$$

Using Eq. (17), the flexural stiffness of the specimens tested in this study was calculated based on both full-composite and partial-composite actions as presented in Table 3. It shows that none of the sandwich specimens tested in this study exhibited full-composite action. For example, the flexural stiffness of Specimen G2-S300 was calculated 64.93 N-m^2 based on the partial-composite action. On the other hand, the flexural stiffness of the specimen obtained from the moment-curvature and ASTM D7250 methods are 70.98 and 53.86 N-m^2. The analytical flexural

stiffness of 64.93 N-m^2 based on the partial-composite action is only 0.8% larger than the average experimental value is 64.42 N-m^2, which indicates a very good agreement. At the same time, the full-composite action results in an flexural stiffness of 134.12 N-m^2, which is much larger than both experimental and partial-composite action values. A degree of full-composite action can also be defined as the ratio of D'/D or $1/(k+1)$. As shown in Table 3, for Specimen G1-S300 and G2-S300, the degree of full-composite action is 91 and 48%, respectively. It means adding one layer of GFRP to each face made the facesheets too stiff compared to the core and changed the behavior of the specimens as observed in the experimental program. The same calculations were performed for G1-S150 and G2-S150 specimens resulted in an degree of full-composite action of 35 and 15%, respectively. It indicates that the shear deformations of the core in the longitudinal direction affect the composite action of the short specimens more than long specimens. It is logical as the top and bottom facesheets have less length to transfer the longitudinal forces causing more shear stress in the core. It should be highlighted that there is a significant difference between the flexural stiffness of the short specimens obtained from the experimental and analytical methods. The difference might be due to the shear contribution of facesheets, which is typically ignored in theory of sandwich composites.

5.3. Effect of Core Shear Modulus

In this section, the results of a parametric study on the effect of core shear modulus on the degree of full-composite action of the test specimens is presented. The core shear modulus was changed from almost zero to 200 MPa. As shown in Figure 16, the core shear modulus has a major effect on the behavior of sandwich composites. For example, if the core shear modulus increased from the average experimental value of 16.6 MPa to 33.2 MPa (100% increase), the degree of full-composite action of G1-S300 and G2-S300 would increase 9 and 54%, respectively. Overall, it

can be concluded that the 3D core used in the current study can provide a shear modulus enough for the sandwich beams with one-layer GFRP facesheets and 300 mm span to develop 91% full-composite action. For thicker facesheets and/or shorter spans, the 3D core does not provide enough shear modulus for full-composite action and a partial-composite action must be considered for design applications.

5.4. Effect of Overhang Length

As the specimens tested in this study had a constant overhang (cantilevered) length of 25 mm, a parametric study on the effect of the overhang length was performed. The overhang length was changed from an extreme case of zero to 50 mm. The mid-span deflection of the specimens was computed based on the solution of thick facesheet sandwich beams per Allen [5]. The deflections were normalized with the corresponding deflection of zero overhang to compare the behavior of the specimens. Figure 17 presents the normalized mid-span deflection of the test specimens against the overhang length. The figure shows that as the overhang length increases the normalized deflection decreases. However, after a certain overhang length, the normalized deflection approaches to a constant value. It cab be observed that the short span specimens (S=150 mm) are more sensitive to the overhang length than the longer ones (S=300 mm). Also, the specimens with two layers of GFRP facesheets are affected more than the specimens with one layer of GFRP facesheets. As shown in Figure 17, the overhang length of 25 mm for the specimens tested in this study was almost long enough to prevent the effect of short overhangs.

6. CONCLUSION

In this study, small-scale sandwich beams manufactured with GFRP facesheets and a 3D woven fabric core were tested and analyzed. A total of 30 specimens were considered, with either zero,

one, and two facesheets and two span lengths of 150 mm and 300 mm. The load-deflection behavior, load-strain behavior, moment-curvature behavior, and neutral axis location were analyzed. Based on the test results, the flexural stiffness, shear stiffness, core shear modulus of the sandwich beams were calculated. Also, an analytical model was presented to consider the effect of core shear modulus on deformation and composite action of the test specimens. The model is capable to quantify the degree of composite action based on the geometry and material properties of sandwich beams. The sandwich beams tested in this study displayed a partial-composite behavior raging from 15 to 91% of full-composite behavior, which was a function of the relative stiffness of the facesheets and the core plus the length of the shear span. Overall, it can be concluded that this specific 8 mm 3D core is a viable option for the use in sandwich structures, especially where a curved-shape sandwich is needed. However, it must be noted that the compatibility between the facesheet and core materials is crucial and this study illustrated that adding a second layer of GFRP compromised the structural behavior of the sandwich beams due to excessive shear deformation. This was theorized to be caused by an increase in shear deformation in the core in the longitudinal direction of the beam. As a result, the two facesheets began to behave partially independent and the cross-section of the beam was no longer considered with a full-composite action. More studies are needed on larger scale specimens and curved-shape geometries to fully understand the behavior of the 3D fabric cores in sandwich structures. The results will be used for the design of thin-walled sandwich liners for the rehabilitation of underground infrastructure including existing highway culverts and large diameter drainage systems.

7. AKNOWLEDGEMENT

The authors of this paper would like to acknowledge the efforts of the technicians at Dalhousie University's Civil and Resource Engineering Department, Jesse Keane and Brian Kennedy, who helped immensely with the setup, instrumentation and testing process. In addition, the authors acknowledge the National Science and Engineering Research Council of Canada (NSERC) for the Undergraduate Student Research Award (USRA) for the first author and QuakeWrap Inc. (Tucson, AZ, USA) for providing the fiberglass and 3D fabrics as well as the epoxy resin used in specimen fabrication.

8. REFERENCES

[1] Reis EM, Rizkalla SH. Material characteristics of 3-D FRP sandwich panels. Construction and Building Materials. 2008 Jun 30;22(6):1009-18.

[2] Roberts, J. C., M. P. Boyle, P. D. Wienhold, and G. J. White. Buckling, collapse and failure analysis of FRP sandwich panels. Composites Part B: Engineering. 2002;33(4):315-324.

[3] Fam, A, Tarek S, and Sadeghian P. "Fiber element model of sandwich panels with soft cores and composite skins in bending considering large shear deformations and localized skin wrinkling." Journal of Engineering Mechanics. 2016;142(5):04016015.

[4] Sadeghian P, Hristozov D, Wroblewski L. Experimental and analytical behavior of sandwich composite beams: Comparison of natural and synthetic materials. Journal of Sandwich Structures & Materials. 2018 Mar.; 20(3):287–307.

[5] Allen HG. Analysis and design of structural sandwich panels, 2013, Pergamon Press, oxford, UK.

[6] Mathieson, H, and Fam A. "Effect of internal ribs on fatigue performance of sandwich panels with GFRP skins and polyurethane foam core." Journal of Materials in Civil Engineering, 2013, 27(2):A4014005.

[7] Wadley HN, Fleck NA, Evans AG. Fabrication and structural performance of periodic cellular metal sandwich structures. Composites Science and Technology. 2003 Dec 31;63(16):2331-43.

[8] Chou S, Chen HC, Wu CC. BMI resin composites reinforced with 3D carbon-fibre fabrics. Composites science and technology. 1992 Jan 1;43(2):117-28.

[9] Brandt J, Drechsler K, Arendts FJ. Mechanical performance of composites based on various three-dimensional woven-fibre preforms. Composites Science and Technology. 1996 Jan 1;56(3):381-6.

[10] Bannister MK, Braemar R, Crothers PJ. The mechanical performance of 3D woven sandwich composites. Composite Structures. 1999 Dec 31;47(1):687-90.

[11] Mouritz AP, Bannister MK, Falzon PJ, Leong KH. Review of applications for advanced three-dimensional fibre textile composites. Composites Part A: applied science and manufacturing. 1999 Dec 31;30(12):1445-61.

[12] Wang B, Wu L, Jin X, Du S, Sun Y, Ma L. Experimental investigation of 3D sandwich structure with core reinforced by composite columns. Materials & Design. 2010 Jan 31;31(1):158-65.

[13] Khokar N, Biteam AB. Woven 3D fabric material. United States patent US 6,338,367. 2002 Jan 15.

[14] Van Vuure AW, Ivens JA, Verpoest I. Mechanical properties of composite panels based on woven sandwich-fabric preforms. Composites Part A: Applied Science and Manufacturing. 2000 Jul 1;31(7):671-80.

[15] Zhang H, Kuang N, Sun F, Fan H, Wang X. Ultra-light CRH wind deflector fabricated by woven lattice sandwich composites. Composites Science and Technology. 2014 Oct 6;102:145-51.

[16] Van Vuure AW, Pflug J, Ivens JA, Verpoest I. Modelling the core properties of composite panels based on woven sandwich-fabric preforms. Composites Science and Technology. 2000 Jun 1;60(8):1263-76.

[17] Fan H, Zhou Q, Yang W, Jingjing Z. An experiment study on the failure mechanisms of woven textile sandwich panels under quasi-static loading. Composites Part B: Engineering. 2010 Dec 1;41(8):686-92.

[18] Fan H, Yang W, Zhou Q. Experimental research of compressive responses of multi-layered woven textile sandwich panels under quasi-static loading. Composites Part B: Engineering. 2011 Jul 1;42(5):1151-6.

[19] Fan H, Zhao L, Chen H, Kuang N, Yang C, Huang S, Jiang Y. Ductile deformation mechanisms and designing instructions for integrated woven textile sandwich composites. Composites Science and Technology. 2012 Jul 23;72(12):1338-43.

[20] Zhao L, Zheng Q, Fan H, Jin F. Hierarchical composite honeycombs. Materials & Design. 2012 Sep 1;40:124-9.

[21] Jin F, Chen H, Zhao L, Fan H, Cai C, Kuang N. Failure mechanisms of sandwich composites with orthotropic integrated woven corrugated cores: experiments. Composite Structures. 2013 Apr 1;98:53-8.

[22] Fan H, Chen H, Zhao L, Zhou J, Jin F, Zheng J, Kuang N. Flexural failure mechanisms of three-dimensional woven textile sandwich panels: Experiments. Journal of Composite Materials. 2014 Mar;48(5):609-20.

[23] Fan H, Ouyang J, Sun F, Yu P, Kuang N, Hu Y. Light-Weight Design of CRH Wind Deflector Panels based on Woven Textile Sandwich Composites. Acta Mechanica Solida Sinica. 2016 Apr 1;29(2):208-20.

[24] Hu Y, Li W, Fan H, Sun F, Ouyang J, Qu Z, Kuang N. Experimental investigations on the failures of woven textile sandwich panels. Journal of Thermoplastic Composite Materials. 2017 Feb;30(2):196-224.

[25] Fan H, Zhao L, Chen H, Zheng J, Jiang Y, Huang S, Kuang N, Ye C. Dynamic compression failure mechanisms and dynamic effects of integrated woven sandwich composites. Journal of Composite Materials. 2014 Feb;48(4):427-37.

[26] Chen H, Zheng Q, Wang P, Fan H, Zheng J, Zhao L, Jin F. Dynamic anti-crushing behaviors of woven textile sandwich composites: Multilayer and gradient effects. Journal of Composite Materials. 2015 Oct;49(25):3169-79.

[27] Van Vuure AW, Verpoest I, Ko FK. Sandwich-fabric panels as spacers in a constrained layer structural damping application. Composites Part B: Engineering. 2001 Jan 1;32(1):11-9.

[28] Vaidya UK, Hosur MV, Earl D, Jeelani S. Impact response of integrated hollow core sandwich composite panels. Composites Part A: Applied Science and Manufacturing. 2000 Aug 1;31(8):761-72.

[29] Shiah YC, Tseng L, Hsu JC, Huang JH. Experimental characterization of an integrated sandwich composite using 3D woven fabrics as the core material. Journal of Thermoplastic Composite Materials. 2004 May;17(3):229-43.

[30] Betts D, Sadeghian P, Fam A. Experimental Behavior and Design-Oriented Analysis of Sandwich Beams with Biobased Composite Facings and Foam Cores. ASCE Journal of Composites for Construction, 2018 June;22(4):04018020.

[31] Chen J. Predicting progressive delamination of stiffened fibre-composite panel and repaired sandwich panel by decohesion models. Journal of Thermoplastic Composite Materials. 2002 Sep;15(5):429-42.

[32] ASTM D3039. Standard Test Method for Tensile Properties of Polymer Matrix Composite Materials, West Conshohocken, PA, USA: ASTM International, 2008.

[33] Daniel IM, Ishai O, Daniel IM, Daniel I. Engineering mechanics of composite materials. New York: Oxford university press; 1994 Jan.

[34] ASTM D7249. Standard test method for facing properties of sandwich constructions by long beam flexure. West Conshohocken, PA, USA: ASTM International, 2012.

[35] ASTM D7250. Standard practice for determining sandwich beam flexural and shear stiffness. West Conshohocken, PA, USA: ASTM International, 2012.

Table 1. Test Matrix

Case #	Specimen ID	Number of GFRP layers	Span (mm)
1	G0-S150	0	150
2	G0-S300	0	300
3	G1-S150	1	150
4	G1-S300	1	300
5	G2-S150	2	150
6	G2-S300	2	300

Note: Five identical specimens per case were tested.

Table 2. Summary of Test Results.

Case #	Specimen ID	Peak load (N)		Initial stiffness, K (N/mm)		Deflection at peak load (mm)		Peak moment (N-m)		Flexural stiffness, D (N-m^2)		Curvature at peak moment (1/km)		Failure Mode
		AVG	SD	AVG	SD	AVG	SD	AVG	SD	AVG	SD	AVG	SD	
1	G0-S150	221.9	53.0	52.75	0.72	4.45	1.01	6.81	1.63	7.03	0.73	859	166	CC
2	G0-S300	215.8	54.7	8.02	0.86	28.66	6.66	12.89	3.56	4.61	0.45	1871	989	CC
3	G1-S150	1424.6	312.8	230.06	57.87	21.10	5.54	43.71	9.60	48.15	5.15	1627	262	TS
4	G1-S300	1323.9	148.1	71.06	6.97	34.92	3.14	81.24	8.70	61.36	3.94	1396	205	TS
5	G2-S150	1572.9	90.0	182.92	10.06	31.45	4.17	48.26	2.76	46.82	10.28	2653	554	LS
6	G2-S300	628.3	39.6	49.85	3.76	33.67	1.30	38.55	2.43	70.98	5.26	851	59	LS

Notes: AVG= Average; SD= Standard Deviation; CC= Core Crushing; TS= Transverse Shear; LS= Longitudinal Shear

Table 3. Experimental and analytical flexural stiffness of sandwich specimens considering both full- and partial-composite actions

Specimen ID	Flexural stiffness, D (N-m^2)					Degree of full-composite action (%)
	Experimental			Analytical		
	Moment-curvature method	ASTM D7250 method	Average	Partial-composite action	Full-composite action	
G1-S150	48.15	74.76	61.46	18.90	54.03	35
G1-S300	61.36	74.76	68.06	48.99	54.03	91
G2-S150	46.82	53.86	50.34	20.70	134.12	15
G2-S300	70.98	53.86	62.42	64.93	134.12	48

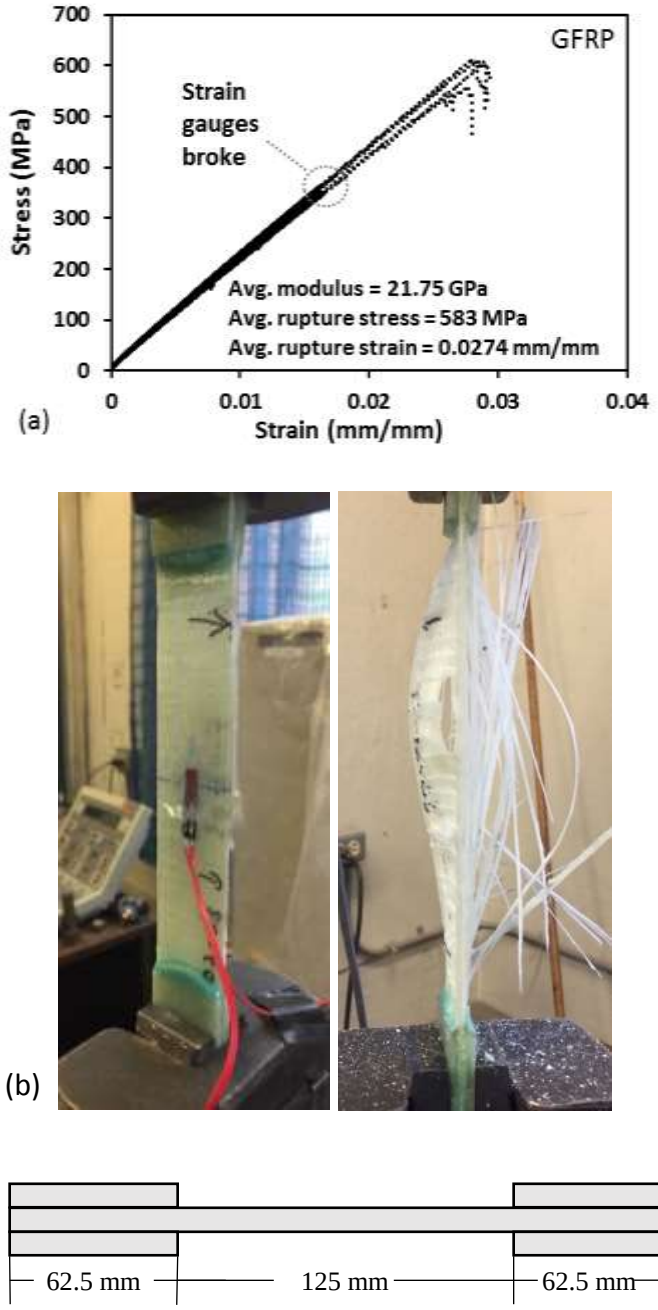

Figure 1. Testing GFRP facing in tension: (a) stress-strain curves; (b) coupon before and after testing; and (c) dimensions.

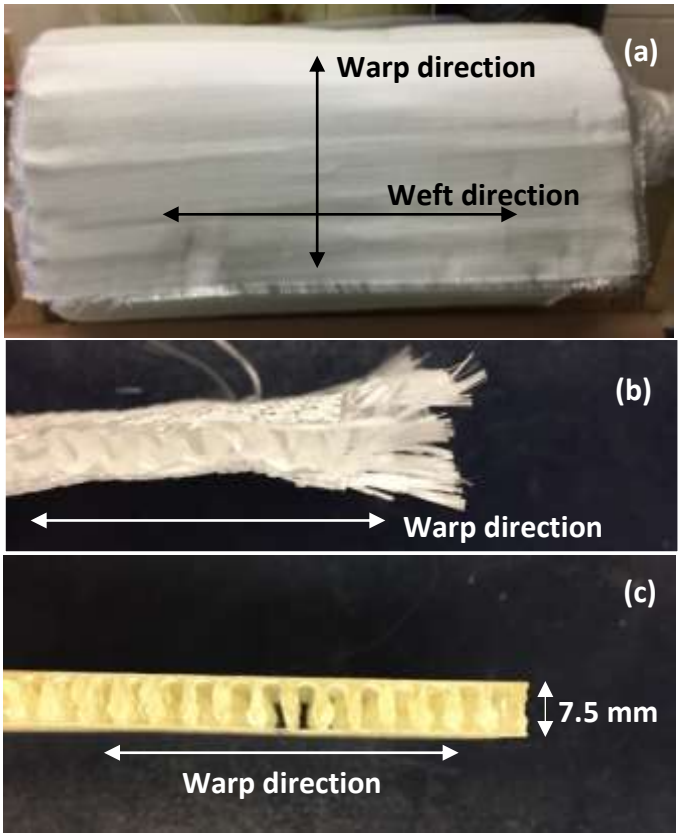

Figure 2. The 3D core used in this study: (a) dry fabric roll; (b) dry fabric layer; and (c) cured with resin.

Figure 3. Fabricated specimens: (a) G1-S300 specimen; and (b) complete test matrix.

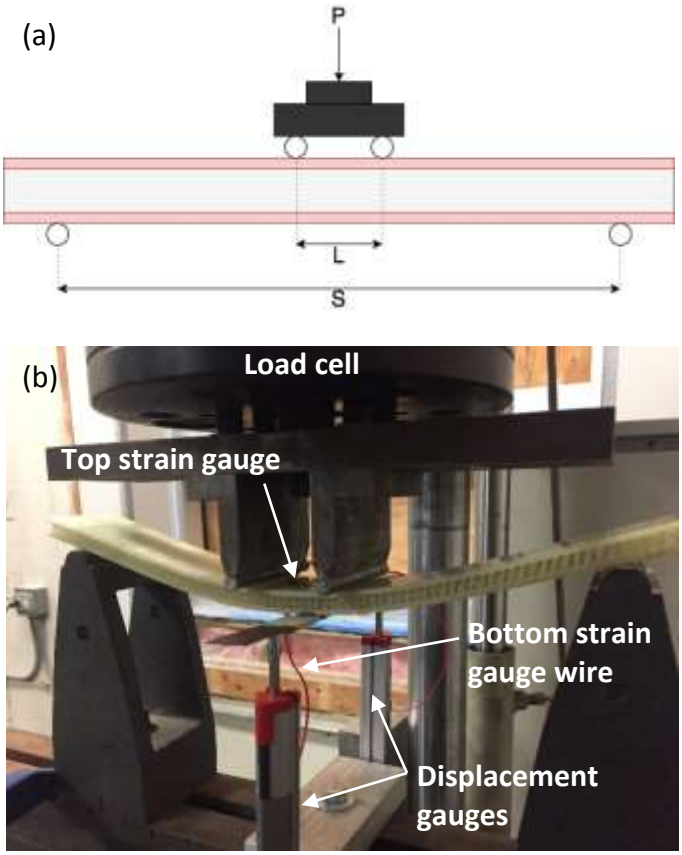

Figure 4. Four-point bending test set-up: (a) schematic; and (b) photo of 300 mm span specimen.

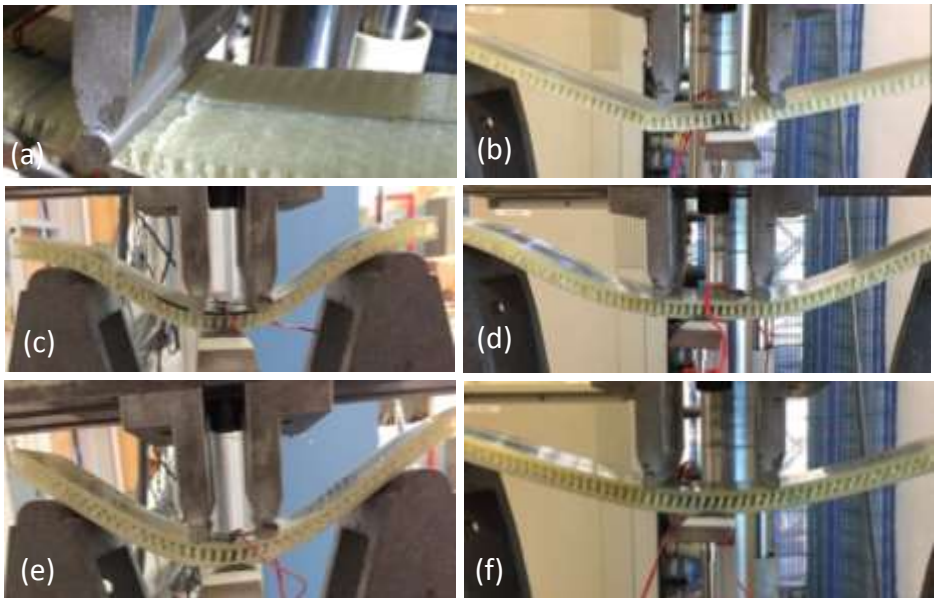

Figure 5. Modes of failure: (a) G0-S150 core crushing; (b) G0-S300 core crushing; (c) G1-S150 transverse shear; (d) G1-S300 transverse shear; (e) G2-S150 longitudinal shear; and (f) G2-S300 longitudinal shear.

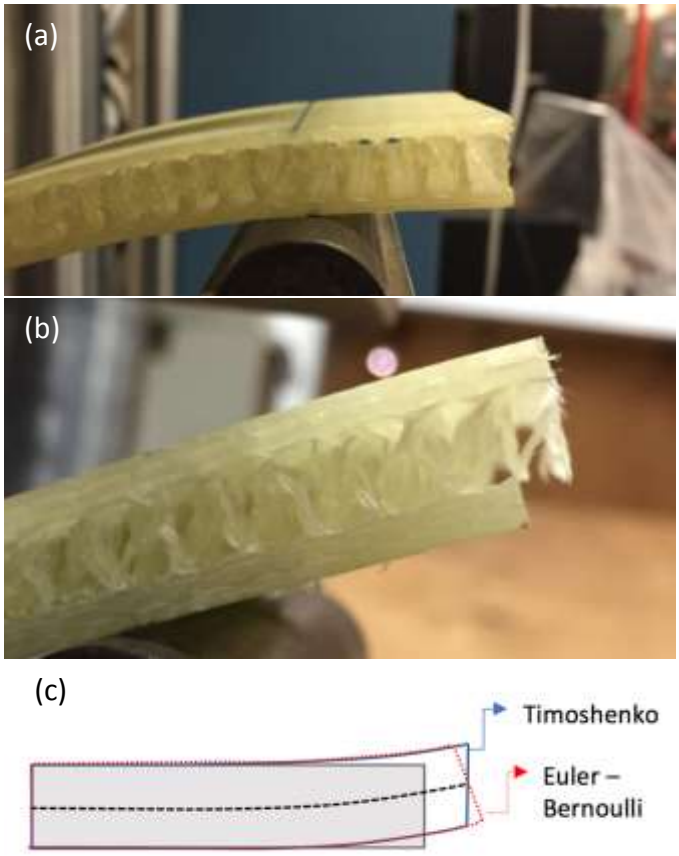

Figure 6. Core shear failure detail: (a) transverse; (b) longitudinal; and (c) theoretical comparison.

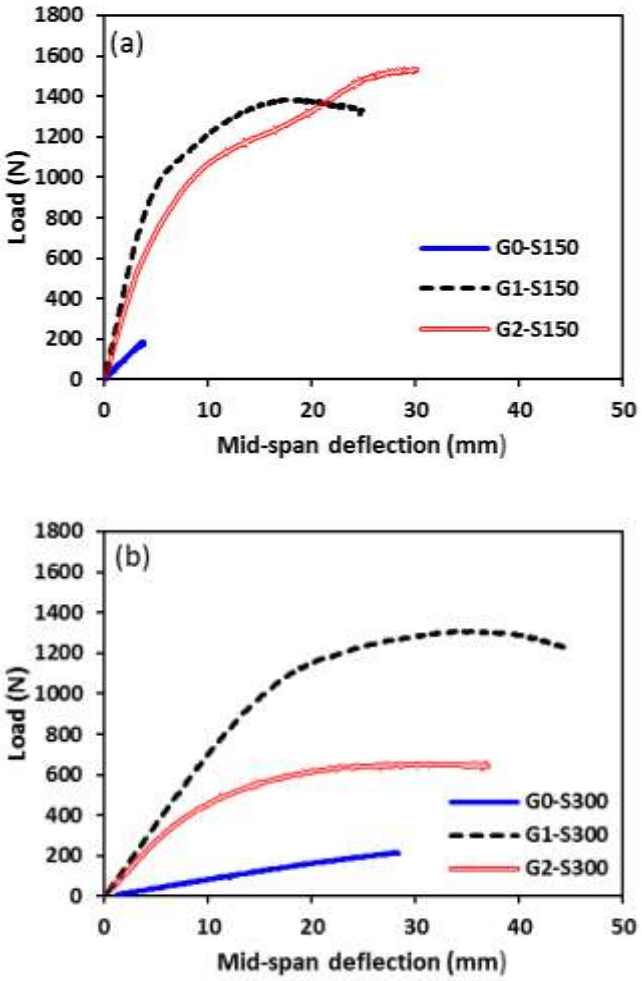

Figure 7. Average load-deflection diagrams: (a) 150 mm span; and (b) 300 mm span (Note: each curve is the average of five identical specimens).

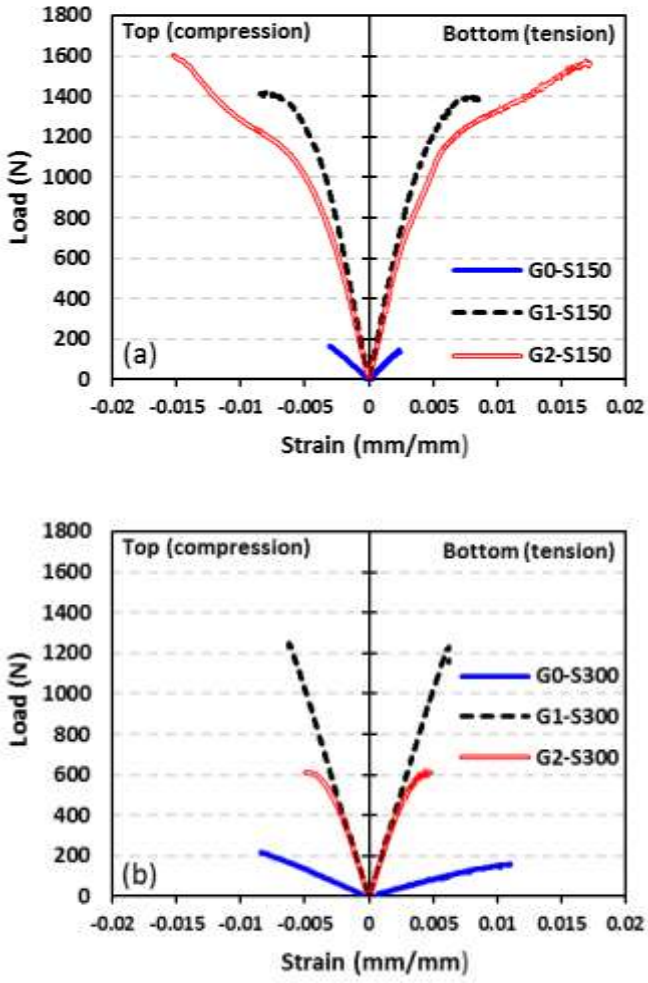

Figure 8. Average load-strain diagrams: (a) 150 mm span; and (b) 300 mm span (Note: each curve is the average of five identical specimens).

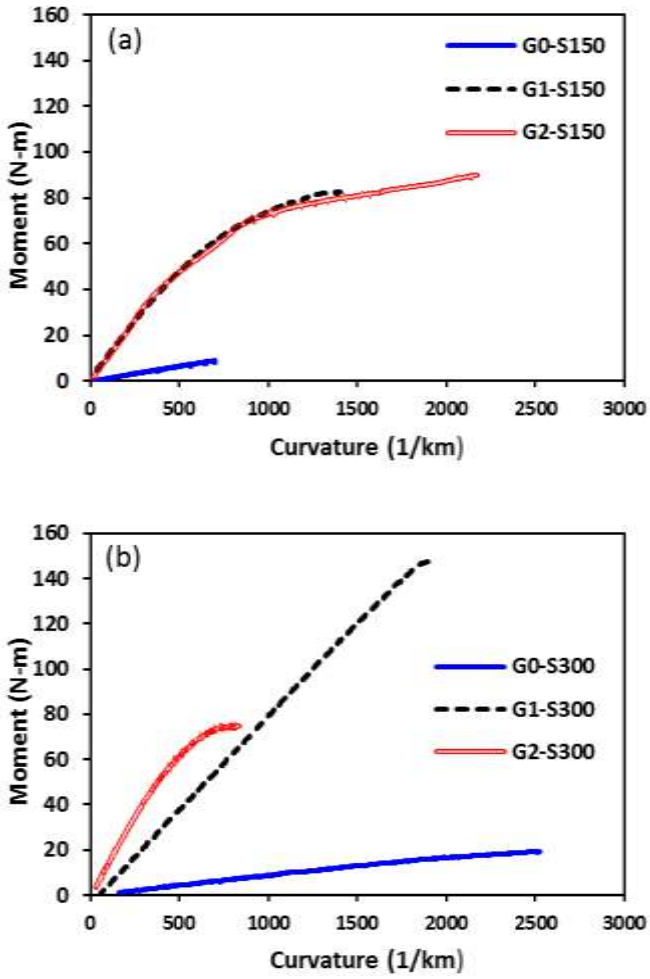

Figure 9. Average moment-curvature diagrams: (a) 150 mm span; and (b) 300 mm span (Note: each curve is the average of five identical specimens).

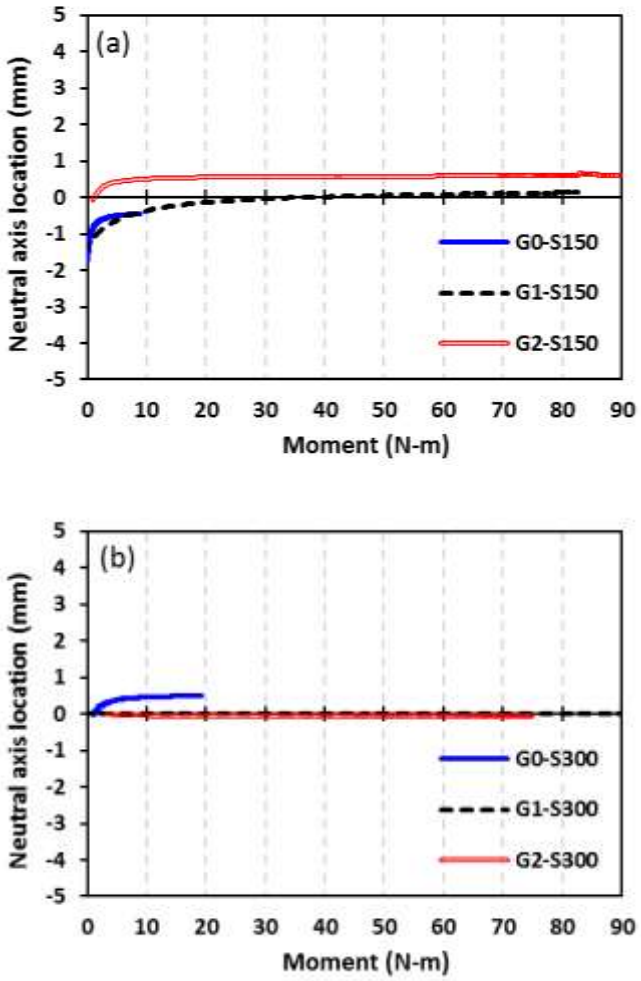

Figure 10. Average neutral axis location vs. moment diagrams: (a) 150 mm span; and (b) 300 mm span (Note: each curve is the average of five identical specimens).

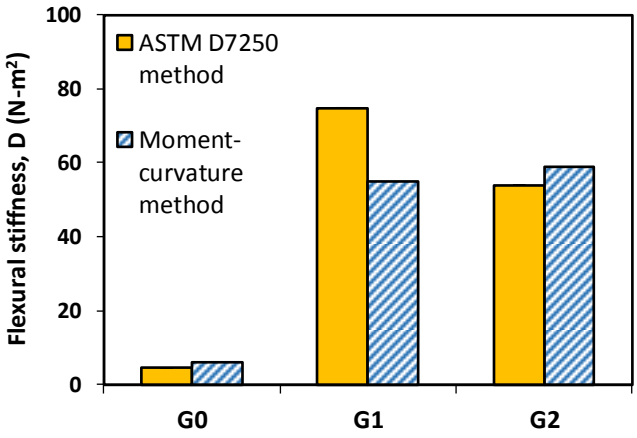

Figure 11. Comparison of experimental flexural stiffness of sandwich composites based on moment-curvature and ASTM D7250 methods.

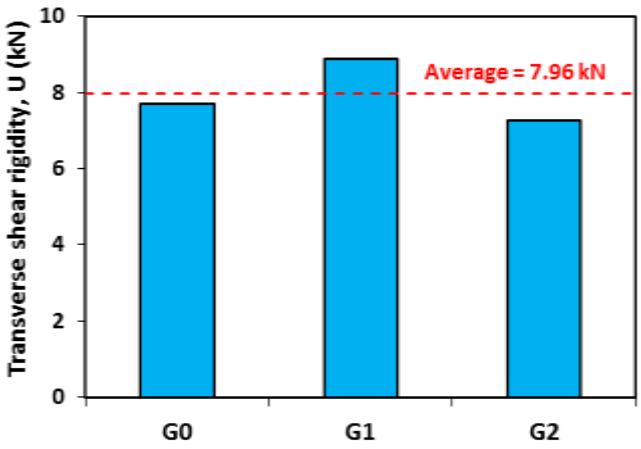

Figure 12. Variation in experimental shear stiffness of sandwich composites based on ASTM D7250 method.

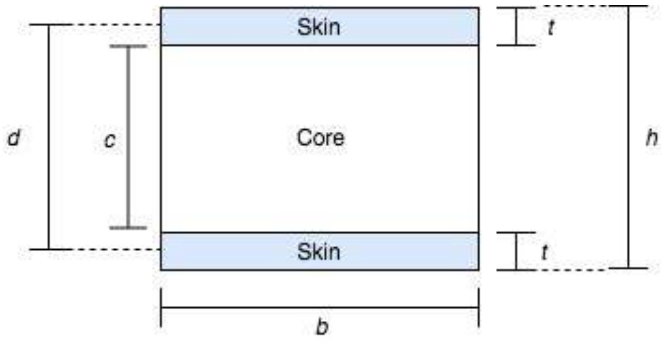

Figure 13. Sandwich beam cross section schematic.

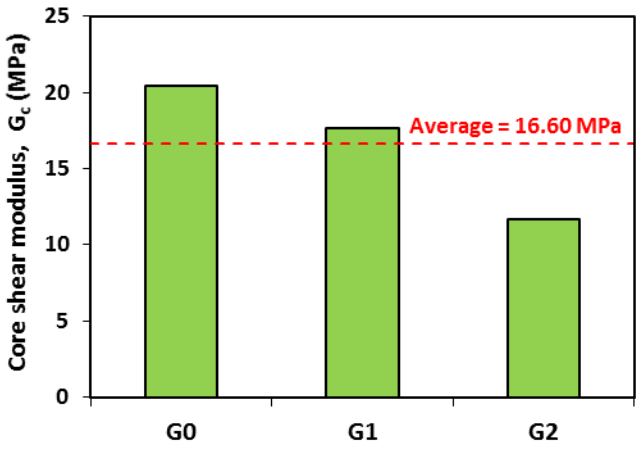

Figure 14. Variation in core shear modulus of sandwich composites calculated from experimental shear stiffness.

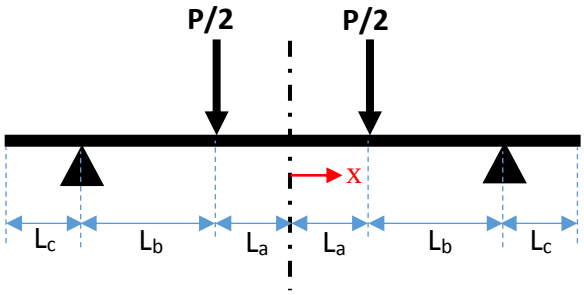

Figure 15. Beam model under four-point bending formulizing partial composite action.

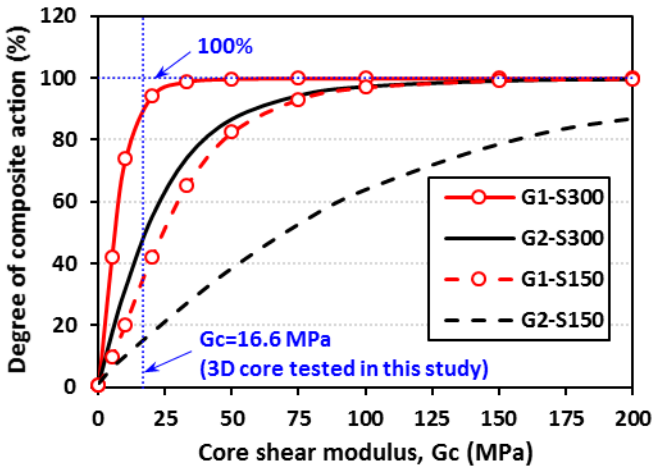

Figure 16. Effect of core shear modulus on composite action of test specimens.

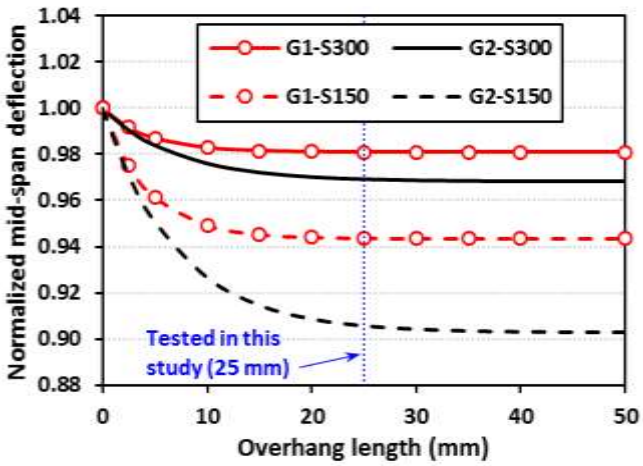

Figure 17. Effect of overhang length on normalized mid-span deflection of test specimens via a parametric study.